Robust LQR control for stall flutter suppression: A polytopic approach

Fabien Niel, Alexandre Seuret, Luca Zaccarian, Casey Fagley

Robust LQR control for stall flutter suppression: A polytopic approach ⋆

Fabien Niel [*,**] **Alexandre Seuret** [*] **Luca Zaccarian** [*,***]
Casey Fagley [**]

[*] *Laboratory for Analysis and Architecture of Systems, Methods and Algorithms for Control, Toulouse, 31031 France (e-mail: fabien.niel.af@gmail.com).*
[**] *Department of Aeronautics, U.S. Air Force Academy, CO 80840, USA.*
[***] *Dept. of Industrial Engineering, University of Trento, Italy.*

Abstract: In this paper, a robust Linear quadratic regulator (LQR) of a NACA 0018 wing with a flap actuator is developed for stall flutter suppression. The nonlinear and switched set of equations of the aeroelastic model is detailed and conveniently expressed as a polytopic uncertain system. The model is then derived to obtain a Linear matrix inequalities (LMIs) formulation of the LQR problem in the presence of uncertainties. The problem is then solved and the arising solutions are presented.

Keywords: Robust control applications, Uncertain dynamic systems, Robust linear matrix inequalities

1. INTRODUCTION

Over the year, improvements in aeronautical technologies, especially in terms of structure, have permitted to obtain more efficient and lighter designs. However, these structures are usually more flexible and are more sensitive to unforeseen aerodynamic conditions and aeroelastic instabilities. These instabilities, such as *flutter*, can be extremely destructive as the high altitude, long endurance prototype of flying wing Helios unfortunately experienced, see Noll et al. (2004). For this reason, these phenomena have been widely studied over the past decades to obtain a better comprehension of these interactions as it can be found in McCroskey et al. (1976); Dimitriadis and Li (2009); Razak et al. (2011) among many others.

Two different types of flutter have been identified which are known as *classical flutter* and *stall flutter*.

- *Classical flutter* is an unstable mode of the wing involving coupled oscillations of pitch and plunge resulting from the coupling between the structural mode and aerodynamic loads. Classical flutter is well represented by a linear fluid-structural model, and has therefore been readily integrated into a variety of controls approaches.
- *Stall flutter* results from a coupling between the nonlinear and unsteady process of *Dynamic stall*, where the flow alternatively separates from the wing and reattaches, and the torsional mode of the wing. This phenomenon leads to the apparition of oscillations, limited in amplitude, known as Limit cycle oscillations (LCO). *Stall flutter* can be experienced with only one degree of freedom, and primarily relies upon the coupling with unsteady vorticity generation and convection in the flow. Details can be found in Fagley et al. (2016).

Modeling these nonlinear phenomena remains extremely challenging, especially including the *dynamic stall*. Numerous of models have been developed such as the different works in Leishman (2006), (Dat et al., 1979). Among them, two particular models are of interest. Based on Goman and Khrabrov (1994), recent adaptation of the G-K model presented in the work by Williams et al. (2015) with only a few number of states and identified parameters adequately represents the dynamic stall behavior. This work, combined with the work of Truong in Truong (1993), accurately predicts the lift and moment coefficient during the pitching motion of a wing. The development of this model has been detailed in Niel et al. (2017).

The aerodynamic model can then be coupled to the structural dynamics of the wing to obtain an nonlinear aeroelastic model which accurately describes LCO behavior present with *stall flutter*. In particular, *stall flutter* has been addressed in several works using active flow control. In Li et al. (2016), a *dynamic stall* model for rotating blade is derived from Beddoes-Leishman. An adaptive controller is designed and simulated for various flutter conditions. In Prime et al. (2010), an LPV-LQR controller is synthesized to suppress the LCO from *stall flutter*. The resulting

⋆ This material is based on research sponsored by the US Air Force Academy under agreement number FA7000-13-2-0002 and FA7000-13-2-0009. The authors would like to acknowledge funding from Dr. Douglas Smith through the Air Force Office of Scientific Research Flow Control and Interaction portfolio. The grant of computer resources by the DoD HPCMO is gratefully acknowledged. The views and conclusions contained herein are those of the authors and should not be interpreted as necessarily representing the official policies or endorsements, either expressed or implied, of the French and US Air Force Academies or the French and U.S. Governments.

auto-scheduled controller displays marginal robustness to airspeed variations. In Haghighat et al. (2014), a mixed norm $\mathcal{H}_2 \setminus \mathcal{H}_\infty$ robust controller is designed. The model used is derived from the ONERA *dynamic stall* model in (Dat et al., 1979).

In this work, the problem of flutter suppression is addressed for a one degree of freedom pitching wing. In Section II , an aeroelastic model adapted from Williams et al. (2015) and Truong (1993) is described. The set of equations is then formulated as a polytopic uncertain system in Section III. After presenting some background on LQR formulation using Linear Matrix Inequalities (LMIs), Section IV presents a polytopic formulation of the problem. In section V, the problem is solved and simulated for a NACA 0018 wing in *stall flutter* conditions. Finally, remarks and conclusions are provided in the final section.

2. AEROELASTIC MODEL

In this section, the aeroelastic model of a pitching wing equipped with a trailing edge flap is presented. This one degree of freedom model will then be studied to address the phenomenon of *stall flutter*.

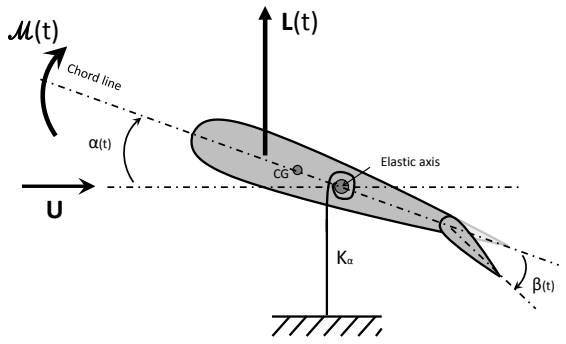

Fig. 1. Model of the pitching equipped with a flap.

As depicted on Fig.1, the wing is pitching at the middle of the chord. In this figure, α represents the pitching angle, or angle of attack, β is the flap deflection angle, U is the freestream velocity. CG is the center of gravity. L corresponds to the lift, and $\mathcal{M}$ represents the pitching moment, conventionally positive for the nose pitching up. The coefficient of moment $C_M = \frac{2\mathcal{M}}{\rho S c U^2}$ is introduced where ρ S and c are the freestream density, the wing surface area and the chord of the wing, respectively.

The linearized equation of motion of the wing is given by:

$$I_\alpha \ddot{\alpha} + C_\alpha \dot{\alpha} + K_\alpha \alpha = \mathcal{M} \tag{1}$$

where with K_α is the torsional stiffness, C_α is the torsional damping and I_α is the inertia around the center of rotation. $\mathcal{M}$ represents the total moment at the center of mid-chord and is split in three components such as

$$\mathcal{M} = \mathcal{M}_w + \mathcal{M}_\beta + \mathcal{M}_{ext} \tag{2}$$

where $\mathcal{M}_w$ represents the aerodynamic moment produced by the wing, $\mathcal{M}_\beta$ is the aerodynamic moment produced by the flap. $\mathcal{M}_{ext}$ is the exterior moment which can eventually be applied. This can correspond for example to the torque produced by an electrical motor connected to the axis of rotation.

2.1 Dynamic hysteresis aerodynamic model

The model of the aerodynamic moment produced by the wing without actuation is adapted from Williams et al. (2015). In this work, derived from Goman and Khrabrov (1994), the lift or the moment coefficients are related to the dynamics of the location of the separation point, denoted x_s and such that

$$x_s \in [0, 1]. \tag{3}$$

This point corresponds to the distance from the leading edge, normalized by the chord length, where the flow is separated from the wing. Thus, picking $x_s = 0$ corresponds to a fully separated flow while $x_s = 1$ represents a fully attached flow. The dynamic of this point follows a first order equation:

$$\tau_1 \dot{x}_s = -x_s + x_{s,0}(\alpha - \tau_2 \dot{\alpha}) \tag{4}$$

where τ_1 and τ_2 are two constants and function $x_{s,0}$ corresponds to the static separation point location, which can be modeled as a function of the angle α and its derivative $\dot{\alpha}$. The function $x_{s,0}$ can be evaluated experimentally using quasi static data.

The moment produced by the wing is then given by (5).

$$\mathcal{M}_w = \frac{1}{2}\rho U^2 S c \left[2\pi\alpha\eta(x_s) + C_{M\text{offset}}\right] \tag{5}$$

where

$$\eta(x_s) = \eta_2 x_s + \eta_1(1 - x_s) \tag{6}$$

and where η_2 and η_1 represent respectively the slope of the moment coefficient for a fully attached and fully detached flow. $C_{M\text{offset}}$ is the offset value of moment coefficient.

***Remark** 1.* The control algorithm derived in this paper is designed by considering the situation where the freestream velocity U may vary in a certain allowable set, but can be approximated by an (unknown) constant parameter during the dynamic evolution. Then, the moment in (5) introduces a constant bias affecting dynamics (1), whose size depends on the constant $C_{M\text{offset}}$ and on the parameter U. When designing our controller we will focus on the unperturbed dynamics resulting from $C_{M\text{offset}} = 0$, but it is clear that the developed results easily extend to the case of constant values of $C_{M\text{offset}}$ and U, because the corresponding effect is merely to shift the equilibrium point.

This model referenced as the GK model proves to be particularly convenient, using a small number of states and constants, and capturing particularly well the hysteresis loop which appears during the dynamic motions as presented on Fig. 2 for example.

2.2 Dynamic stall model

However, due to the vortex shedding that appears in the dynamic motion, specifically in the reattachment cycle, the previous model presents some inaccuracies, especially for rapid motion and/or at high angles of attack. For this reason, this model is extended, including the work in Truong (1993). This work, based on Tobak's work on the Hopf bifurcation in Tobak and Chapman (1985), permits

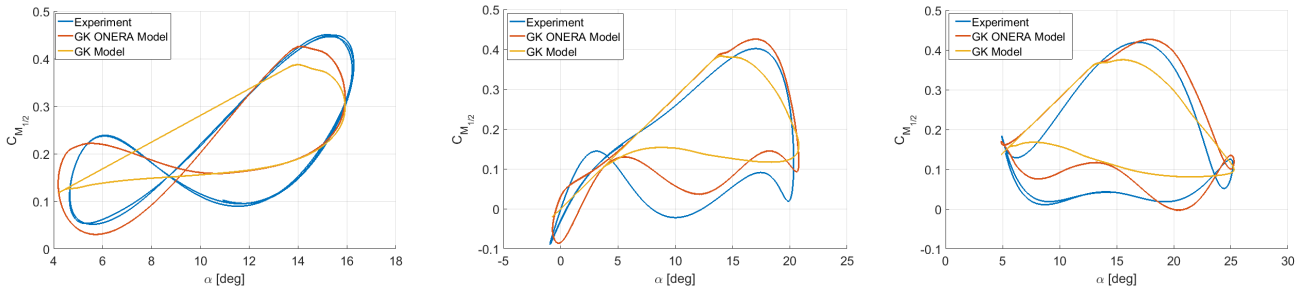

(a) $\alpha_0 = 10^o$, $\alpha_1 = 6^o$, $k = 0.2$. (b) $\alpha_0 = 10^o$, $\alpha_1 = 10^o$, $k = 0.1$. (c) $\alpha_0 = 15^o$, $\alpha_1 = 10^o$, $k = 0.1$.

Fig. 2. Moment coefficients curve predictions and measures for various values of α_0, α_1 (in degrees) and k.

$$A(x, x_s) = \begin{bmatrix} -\frac{C_\alpha}{I_\alpha} & \frac{\pi\rho U^2 Sb\eta(x_s) - K_\alpha}{I_\alpha} & 0 & \frac{\rho U^2 Sb}{2I_\alpha} \\ 1 & 0 & 0 & 0 \\ w_S\left(D_M(x)\frac{C_\alpha}{I_\alpha} - E_M(x)\right) & w_S D_M(x)\left(\frac{\pi\rho U^2 Sb\eta(x_s) - K_\alpha}{I_\alpha}\right) & w_S\beta_M(x) & -w_S\left(w_S + \frac{\rho U^2 Sb}{2I_\alpha}\right) \\ 0 & 0 & 1 & 0 \end{bmatrix}, \quad (7)$$

$$B = \frac{1}{2}\rho U^2 SbC_{M,\beta}\,[1\ 0\ -w_S D_M(x)\ 0]', \quad C(x_s) = \begin{bmatrix} 0 & 2\pi\eta(x_s) & 0 & 1 \\ 0 & 1 & 0 & 0 \end{bmatrix}, \quad F = [0\ 1\ 0\ 0].$$

to predict the oscillatory behavior that can be experienced, especially on the down-stroke of the motion. In Truong (1993), the original model for the moment coefficient is split in a steady and unsteady parts such as:

$$C_M = C_{M_s} + C_{M_u}, \quad (8)$$

where C_{M_s} and C_{M_u} represent respectively the steady and unsteady component of the moment coefficient. In this present work, the precedent formulation of the GK model is preferred to account for the steady component. The unsteady component follows the following simplified second order dynamic:

$$\begin{aligned} \ddot{C}_{M_u} &= w_S\beta_M(\alpha,\dot{\alpha})\dot{C}_{M_u} - w_S^2 C_{M_u} \\ &\quad -E_M(\alpha,\dot{\alpha})w_S\dot{\alpha} - D_M(\alpha,\dot{\alpha})w_S\ddot{\alpha}. \end{aligned} \quad (9)$$

where w_s is a constant, and β_M, E_M and D_M are a set of constant depending on α and $\dot{\alpha}$. Let define α_s, the critical angle of attack and Ω_{up}, the following set:

$$\Omega_{up} := \Omega^1_{up} \cup \Omega^2_{up}$$

where

$$\begin{aligned} \Omega^1_{up} &= \{(\alpha,\dot{\alpha}) \in [-180, 180] \times \mathbb{R}, \alpha \in [-\alpha_s, 0]\ ,\ \dot{\alpha} < 0\} \\ \Omega^2_{up} &= \{(\alpha,\dot{\alpha}) \in [-180, 180] \times \mathbb{R}, \alpha \in [0, \alpha_s]\ ,\ \dot{\alpha} > 0\} \end{aligned}$$

Then, we can now defined β_M, E_M and D_M as a two-valued set of functions such as,

$$\{D_M, \beta_M, E_M\} = \begin{cases} \{D_{M,1}, \beta_{M,1}, E_{M,1}\} & \text{if } (\alpha,\dot{\alpha}) \in \Omega_{up}, \\ \{D_{M,2} = 0, \beta_{M,2} < 0, E_{M,2} = 0\} & \text{elsewhere} \end{cases}$$

where parameters $D_{M,i}$, $\beta_{M,i}$ and $E_{M,i}$, for $i = 1, 2$, are constant and known. The resulting aerodynamic equations for the moment produced by the wing can then be summarized as follows

$$\begin{cases} \mathcal{M}_w &= \frac{1}{2}\rho U^2 Sc\,[2\pi\alpha\eta(x_s) + C_{M\text{offset}} + C_{M_u}], \\ \ddot{C}_{M_u} &= w_S\beta_M(\alpha,\dot{\alpha})\dot{C}_{M_u} - w_S^2 C_{M_u} \\ &\quad -E_M(\alpha,\dot{\alpha})w_S\dot{\alpha} - D_M(\alpha,\dot{\alpha})w_S\ddot{\alpha}, \\ \tau_1\dot{x}_s &= -x_s + x_{s,0}(\alpha,\dot{\alpha}). \end{cases} \quad (10)$$

Experiments have been conducted in the Subsonnic Wind Tunnel of Aeronautics Laboratory of the United States Air Force Academy at an elevation of $7,000ft$. The wind tunnel designed and built by FluiDyne Engineering, is a recirculating tunnel with a 0.91 m by 0.91 m by 1.83 m test section. The freestream velocity was $U_\infty = 22.5m/s$. This resulted in a Mach number of $M = 0.068$ and a chord-based Reynolds number $Re_c = 190.10^3$.

The article used in the experimentation is a rectangular, finite span, NACA 0018 cross sectional wing with a chord of $c = 0.15$ m and a span of $b = 0.45$ m. The wing section oscillates about the mid chord by a circular spar attached to a DC brushless motor which dynamically pitches the wing section.

The resulting pitch oscillation is described as

$$\alpha = \alpha_0 + \alpha_1 sin(kt^+),$$

where we define $k = \frac{2\pi fc}{U_\infty} = \frac{\omega c}{2U_\infty}$ the reduced frequency with $\omega = 2\pi f$ the angular frequency and $t^+ = \frac{t}{t_{conv}}$ the time normalized by the convective time, $t_{conv} = \frac{c}{U}$.

Figure 2 provides examples of the experimentation conducted. A good agreement between the model prediction and experimental results is observed. In particular, the model proposed by Williams successfully captures the hysteresis loop of the coefficient of moment but fails to capture any secondary frequencies due to vortex shedding. Alternatively, the model proposed in this paper reproduces in addition the oscillations during the down-stroke of the motion. More details of this model are provided in Niel et al. (2017).

2.3 Actuator model

The moment produced by the trailing flap is defined by

$$\mathcal{M}_\beta = \frac{1}{2}\rho U^2 ScC_{M,\beta}\beta \quad (11)$$

where

- $C_{M,\beta}$ is a given and known constant,
- β is the flap deflection angle.

Note that the dynamics of the flap actuator is not considered in this work, similarly to Haghighat et al. (2014).

2.4 Complete aeroelastic model

The resulting equations of the complete aeroelastic model of the wing are then given by Eq. (1), (10) and (11). The previous final set of equation can thus be formulated as the non linear system:

$$\begin{aligned} \dot{x} &= A(x, x_s)x + B(x)u \\ \tau_1 \dot{x}_s &= -x_s + x_{s,0}(x) \\ y &= C(x)x \\ z &= Fx \end{aligned} \tag{12}$$

where the vector $x \in \mathbb{R}^4$ is given by

$$x = [\, \dot{\alpha},\, \alpha,\, \dot{C}_{M_u},\, C_{M_u}\,]', \tag{13}$$

and vector $u\ (= \beta)$, y and z are the the control input, the output and the measurement vectors of the system. The matrices A, B, C and F are given in (7) (at the top of the previous page).

System (12) can be seen as a nonlinear switched system, for which a dedicated stability analysis needs to be provided. In order to solve this problem, we will provide in the next section a polytopic model for system (12), for which such an analysis is easier.

3. POLYTOPIC MODELING

As mentioned above, system (12) presents some nonlinearities due to the products in the dynamics of the variable x_s and also to bilinear terms appear with the function $\eta(x_s)$ in the matrix $A(x, x_s)$.

In order to simplify the model, we will rewrite system (12) as a uncertain polytopic system where uncertain parameters are given in the following description.

$\eta(x_s)$: First, in order to suppress the product $\alpha \times \eta$ from the equation, let consider η introduced previously in equation (6). We note that η is a linear combination of the state variable x_s. Since x_s cannot be directly measured, it is reasonable to consider as an uncertainty to the system and use the fact that it lies in the interval $[0,\ 1]$. Therefore parameter η verifies

$$\eta \in [\eta_1,\ \eta_2]. \tag{14}$$

or equivalently, there exists a scalar function $\lambda_1 \in [0, 1]$ such that

$$\eta(x_s) = \lambda_1 \eta_1 + (1 - \lambda_1)\eta_2. \tag{15}$$

E_M, β_M, D_M: Secondly, instead of considering a pure switch of the sets of the constants $\{D_M, \beta_M, E_M\}$ in Eq.(10), a linear variation is conveniently introduced depending on an additional parameter parameter. This technique has been successfully used in Olalla et al. (2009). Therefore, there exists a function $\lambda_2 \in [0, 1]$ such that

$$\begin{aligned} \{D_M, \beta_M, E_M\} := \lambda_2 \{&D_{M,1}, \beta_{M,1}, E_{M,1}\} \\ &+(1 - \lambda_2) \{D_{M,2}, \beta_{M,2}, E_{M,2}\}. \end{aligned} \tag{16}$$

U^2: Finally, matrices A and B also depend on uncertainties. Especially, the free stream velocity U can be considered as uncertain due to the possible gusts of wind that can be encountered during flight, or just because of the uncertainty in its measurement. Therefore, there exists a function $\lambda_3 \in [0, 1]$ such that

$$U^2 = \lambda_3 U_1^2 + (1 - \lambda_3)U_2^2. \tag{17}$$

Even though we assumed that U be constant (and unknown) during motion, and so that quantity λ_3 in (17), we consider a time-varying version of the uncertain vector $\lambda(t) = [\lambda_1(t)\ \lambda_2(t)\ \lambda_3(t)]'$ in $[0\ 1]^3$, comprising the coefficients λ_l, for any $l = 1, 2, 3$, which can vary with time and are not necessarily constant.

Based on this uncertain vector, and the relations in (15)–(17), we can derive a polytopic uncertain model of system (12), corresponding to:

$$\begin{aligned} \dot{x} &= \sum_{i,j,k=1}^{2} \lambda_1^i \lambda_2^j \lambda_3^k \left(A_{i,j,k}x + B_{i,j,k}u\right) \\ &= \sum_{i,j,k=1}^{2} \mu_{ijk} \left(A_{i,j,k}x + B_{i,j,k}u\right) \\ y &= \sum_{i,j,k=1}^{2} \lambda_1^i \lambda_2^j \lambda_3^k C_{i,j,k}x = \sum_{i,j,k=1}^{2} \mu_{ijk} C_{i,j,k}x \\ z &= Fx \end{aligned} \tag{19}$$

where $\lambda_l^1 = \lambda_l(t)$ and $\lambda_l^2 = 1 - \lambda_l(t)$, for $l = 1, 2, 3$, matrices $A_{i,j,k}$, $B_{i,j,k}$ and $C_{i,j,k}$ are given in (18), at the top of the next page, and where we introduced the scalars μ_{ijk}. These scalars, in particular, satisfy $\sum_{i,j,k=1}^{2} \mu_{ijk} = 1$, which reveals that the multiaffine dynamics (12) can be written as a convex combination of $2^3 = 8$ linear time-invariant models corresponding to all possible selections of $i, j, k \in \{0, 1\}$ in (18)(see, e.g., (Belta et al., 2002, Prop. 2) for details).

4. LMI-BASED SELECTION OF AN LQR CONTROLLER

The polytopic model (19) derived in the previous section allows us to apply several different control strategies for the selection of input $u = \beta$, corresponding to the flap deflection angle in Figure 1.

For this preliminary work, we follow the same approach adopted in Olalla et al. (2009), which in turns is based on the LQR design formulation presented in Feron et al. (1992). The objective of that formulation is to select input u in such a way to perform some convex optimization geared towards reducing the cost function

$$J = \int_0^\infty (x'Qx + u'Ru)dt, \tag{20}$$

where R is a positive definite matrix and Q is a positive semi-definite matrix that may be freely selected as long as (Q, A_{ijk}) is detectable for all selections of ijk.

Due to the nonlinear nature of the dynamics and the conservativity of the convex embedding in (19), it is hard to exactly solve the minimization of J in (20), nevertheless, one possible conservative approach that leads to reduced values of J is the one given in Olalla et al. (2009), which is

$$A_{i,j,k} = \begin{bmatrix} -\frac{C_\alpha}{I_\alpha} & \frac{\pi\rho U_k^2 Sb\eta_i - K_\alpha}{I_\alpha} & 0 & \frac{\rho U_k^2 Sb}{2I_\alpha} \\ 1 & 0 & 0 & 0 \\ w_S\left(D_{M,j}\frac{C_\alpha}{I_\alpha} - E_{M,j}\right) & w_S D_{M,j}\left(\frac{\pi\rho U_k^2 Sb\eta_i - K_\alpha}{I_\alpha}\right) & w_S\beta_{M,j} & -w_S\left(w_S + \frac{\rho U_k^2 Sb}{2I_\alpha}\right) \\ 0 & 0 & 1 & 0 \end{bmatrix}, \tag{18}$$

$$B_{i,j,k} = \frac{1}{2}\rho U_k^2 SbC_{M,\beta}\left[1\ 0\ -w_S D_{M,j}\ 0\right]', \quad C_{i,j,k} = \begin{bmatrix} 0 & 2\pi\eta_i & 0 & 1 \\ 0 & 1 & 0 & 0 \end{bmatrix}, \quad F = [0\ 1\ 0\ 0].$$

based on the solution to the following convex optimization problem:

$$\min_{P,Y,X} \mathbf{Tr}QP + X, \text{ subject to:} \tag{21}$$
$$A_{i,j,k}P + PA'_{i,j,k} + B_{i,j,k}Y + Y'B'_{i,j,k} + \mathbb{1} < 0,\ \forall i,j,k$$
$$\begin{bmatrix} X & R^{\frac{1}{2}}Y \\ Y'R^{\frac{1}{2}} & P \end{bmatrix} > 0 \quad P = P' > 0.$$

The resulting LQR controller is given by $u = -Kx$, with $K = YP^{-1}$.

5. SIMULATION RESULTS

Using Eq.(21), a robust controller has been synthesized for the polytopic system (19) defined in Section 3, whose solutions include the solution of the nonlinear multiaffine dynamics (12). The values of the parameters of the considered model are listed in Table 1.

Parameter	Value	Parameter	Value
I_α	0.0037 $Nm/rad/s^2$	S	0.0675 m^2
C_α	0.072 $Nm/rad/s$	ρ	0.9 kg/m^3
K_α	2.78 Nm/rad	$C_{M,\beta}$	1
b	0.45 m	η_1	0.0294
c	0.15 m	η_2	0.2558
D_M^+	0.0455	β_M^+	0.0015
E_M^+	-0.0217	β_M^-	-1.5

Table 1. Model parameters used in the simulation study.

If η and $\{D_M, \beta_M, E_M\}$ values are bounded and known, we need to define the margin of uncertainty of the free stream velocity to ensure some robustness to this parameter. The nominal value selected is 20 m/s. We authorize some variation of $\pm 2.5 m/s$ which provides a variation range $[U_{min}, U_{max}] = [17.5\ m/s, 22.5\ m/s]$.

The weighting matrices of the cost function are selected to ensure that the input vector remains limited in amplitude and a reasonable suppression of the *stall flutter*. The matrices used are consequently $Q = \mathrm{diag}\{1, 1, 0.01, 0.01\}$ and $R = 50$. The convex optimization in Eq.(21), leading to the selection of gain K, is solved using the Robust control toolbox available in MATLAB. In particular, the resulting state feedback gain is:

$$K = [0.1427\ 2.977\ -0.0021\ -0.151]$$

The controller is then tested using the simulation model. To initiate the phenomenon of *stall flutter*, an angle of attack of 10^o is set as initial condition. The results for 3 different airspeeds are presented in Figures 3–5. As already observed in Remark 1, while the controller design was performed without the presence of the external disturbance

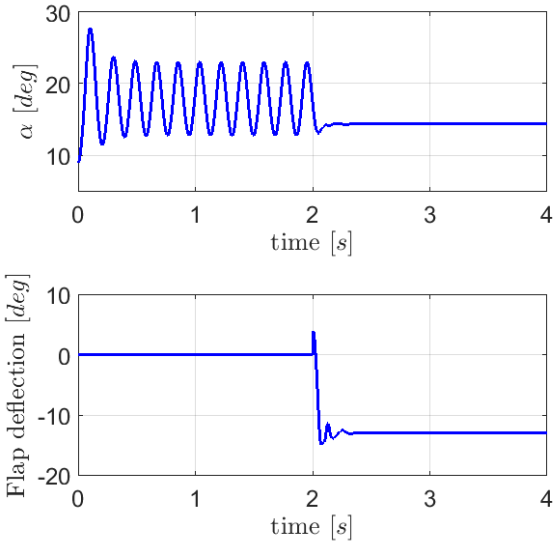

Fig. 3. Angle of attack(^{o}) and flap deflection(^{o}) in function of the time(s) for $U = 20\ m/s$. The controller is activated after 2 s.

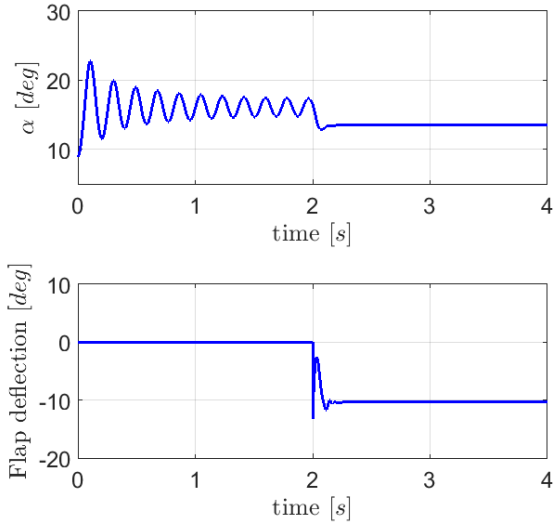

Fig. 4. Angle of attack(^{o}) and flap deflection(^{o}) in function of the time(s) for $U = 17.5\ m/s$. The controller is activated after 2 s.

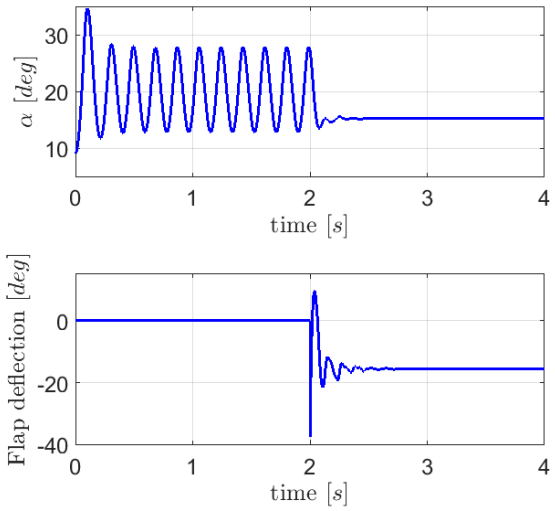

Fig. 5. Angle of attack(^{o}) and flap deflection(^{o}) in function of the time(s) for $U = 22.5\ m/s$. The controller is activated after 2 s.

$C_{M\text{offset}}$, in the simulation we consider a more realistic case of a nonzero value of $C_{M\text{offset}}$ (see Table 1). As expected, the different values of U considered in our three simulations, correspond to different equilibrium points reached by the closed loop.

The simulation results illustrate how the same feedback gain is capable of stabilizing that equilibrium point for the three different values of free stream velocities. The controller successfully suppresses the flutter phenomenon, which is visible in all three simulations, before the controller activation, which always occur at time $t = 2s$.

6. CONCLUSION

In this work, a robust LQR controller for *stall flutter* suppression is designed and computed for a pitching NACA 0018 wing. A non linear and switched aeroelastic model, accounting for the complex phenomenon of *stall flutter*, is presented and conveniently turned as a polytopic uncertain system. A polytopic and LMI formulation of an LQR problem is introduced. The problem is then solved using Matlab. Simulations using the designed controller are then computed. The results for different airspeeds are presented showing that the synthesized controller can successfully suppress the *stall flutter* initially present for the range of variation.

Further work could address the problem of rate or magnitude limitations of the actuator.

REFERENCES

Belta, C., Habets, L., and Kumar, V. (2002). Control of multi-affine systems on rectangles with applications to hybrid biomolecular networks. In *IEEE Conference on Decision and Control*, volume 1, 534–539. IEEE.

Dat, R., Tran, C., and Petot, D. (1979). Modèle phénomènologique de décrochage dynamique sur profil d'hélicoptère. *TP ONERA 1979-149*.

Dimitriadis, G. and Li, J. (2009). Bifurcation behavior of airfoil undergoing stall flutter oscillations in low-speed wind tunnel. *AIAA journal*, 47(11), 2577–2596.

Fagley, C., Seidel, J., and McLaughlin, T. (2016). Cyber-physical flexible wing for aeroelastic investigations of stall and classical flutter. *Journal of Fluids and Structures*, 67, 34–47.

Feron, E., Balakrishnan, V., Boyd, S., and El Ghaoui, L. (1992). Numerical methods for h_2 related problems. In *Proc. American Control Conf*, volume 4, 2921–2922. Citeseer.

Goman, M. and Khrabrov, A. (1994). State-space representation of aerodynamic characteristics of an aircraft at high angles of attack. *Journal of Aircraft*, 31(5), 1109–1115.

Haghighat, S., Sun, Z., Liu, H.H., and Bai, J. (2014). Robust stall flutter suppression using $\mathcal{H}_2/\mathcal{H}_\infty$ control. In *ASME 2014 Dynamic Systems and Control Conference*, V001T01A004–V001T01A004. American Society of Mechanical Engineers.

Leishman, J.G. (2006). *Principles of Helicopter Aerodynamics with CD Extra*. Cambridge university press.

Li, N., Balas, M.J., Yang, H., and Jiang, W. (2016). Flow control and stability analysis of rotating wind turbine blade system. *Journal of Guidance, Control, and Dynamics*.

McCroskey, W., Carr, L., and McAlister, K. (1976). Dynamic stall experiments on oscillating airfoils. *Aiaa Journal*, 14(1), 57–63.

Niel, F., Fagley, C.P., Seidel, J., and McLaughlin, T.E. (2017). Reduced order modeling of a dynamically pitching naca 0018 airfoil. In *55th AIAA Aerospace Sciences Meeting*, 0952.

Noll, T.E., Brown, J.M., Perez-Davis, M.E., Ishmael, S.D., Tiffany, G.C., and Gaier, M. (2004). Investigation of the Helios prototype aircraft mishap volume i mishap report. *Downloaded on*, 9, 2004.

Olalla, C., Leyva, R., El Aroudi, A., and Queinnec, I. (2009). Robust LQR control for pwm converters: an LMI approach. *IEEE Transactions on industrial electronics*, 56(7), 2548–2558.

Prime, Z., Cazzolato, B., Doolan, C., and Strganac, T. (2010). Linear-parameter-varying control of an improved three-degree-of-freedom aeroelastic model. *Journal of Guidance, Control, and Dynamics*, 33(2), 615–619.

Razak, N.A., Andrianne, T., and Dimitriadis, G. (2011). Flutter and stall flutter of a rectangular wing in a wind tunnel. *AIAA journal*, 49(10), 2258–2271.

Tobak, M. and Chapman, G.T. (1985). Nonlinear problems in flight dynamics involving aerodynamic bifurcations. *NASA Technical Memorandum*.

Truong, V.K. (1993). A 2-d dynamic stall model based on a hopf bifurcation. In *European Rotorcraft Forum*, volume 19, C23–C23. Associazione Italiana di Aeronautica ed Astronautica.

Williams, D.R., Reissner, F., Greenblatt, D., Mueller-Vahl, H., and Strangfeld, C. (2015). Modeling lift hysteresis with a modified Goman-Khrabrov model on pitching airfoils. In *45th AIAA Fluid Dynamics Conference*, 2631.